Appl. Math. Mech. -Engl. Ed., **41**(1), 83–104 (2020)

Applied Mathematics and Mechanics (English Edition)

https://doi.org/10.1007/s10483-020-2558-7

Modelling two-layer nanofluid flow in a micro-channel with electro-osmotic effects by means of Buongiorno's model*

M. D. K. NIAZI, Hang XU†

State Key Lab of Ocean Engineering, Collaborative Innovation Center for Advanced Ship and Deep-Sea Exploration (CISSE), School of Naval Architecture, Ocean and Civil Engineering, Shanghai Jiao Tong University, Shanghai 200240, China

(Received Jul. 14, 2019 / Revised Aug. 6, 2019)

Abstract A fully developed steady immiscible flow of nanofluid in a two-layer micro-channel is studied in the presence of electro-kinetic effects. Buongiorno's model is employed for describing the behavior of nanofluids. Different from the previous studies on two-layer channel flow of a nanofluid, the present paper introduces the flux conservation conditions for the nanoparticle volume fraction field, which makes this work new and unique, and it is in coincidence with practical observations. The governing equations are reduced into a group of ordinary differential equations via appropriate similarity transformations. The highly accurate analytical approximations are obtained. Important physical quantities and total entropy generation are analyzed and discussed. A comparison is made to determine the significance of electrical double layer (EDL) effects in the presence of an external electric field. It is found that the Brownian diffusion, the thermophoresis diffusion, and the viscosity have significant effects on altering the flow behaviors.

Key words electrical double layer (EDL), entropy generation, micro-channel, nanofluid

Chinese Library Classification O361

2010 Mathematics Subject Classification 76D05, 76M55, 65D99

Nomenclature

Br_1, Br_2,	Brinkman numbers;
B_0,	magnetic field in z-direction;
$\overline{C}_1, \overline{C}_2$,	nano-particle volume fractions;
C_0,	reference nano-particle volume fraction;
$C_{\rm w}$,	nano-particle volume fraction on the micro-channel walls;
$C_{\rm f1}, C_{\rm f2}$,	local skin friction coefficients;
$(c_p)_{\rm f}, (c_p)_{\rm s}$,	specific heat of fluid and nanoparticles;
$D_{\rm B1}, D_{\rm B2}$,	Brownian diffusion coefficients;
$D_{\rm t1}, D_{\rm t2}$,	thermophoretic diffusion coefficients;
e,	charge of a proton;
$E(m)$,	error for homotopy analysis method (HAM) computation order m;
$E_{\rm s}$,	non-dimensional external electric field parameter;

* Citation: NIAZI, M. D. K and XU, H. Modelling two-layer nanofluid flow in a micro-channel with electro-osmotic effects by means of Buongiorno's model. *Applied Mathematics and Mechanics* (*English Edition*), **41**(1), 83–104 (2020) https://doi.org/10.1007/s10483-020-2558-7

† Corresponding author, E-mail: hangxu@sjtu.edu.cn

Project supported by the National Natural Science Foundation of China (No. 11872241)

E_x, E_y,	electric field in x- and y-directions respectively;
F_1, F_2,	electrical body forces from uniform electromagnetic field;
H,	total distance between the boundaries of the channel;
H_1, H_2,	distances of two-layer fluid in Regions Ⅰ and Ⅱ;
h_1, h_2,	non-dimensional distances of Regions Ⅰ and Ⅱ;
Ha_1, Ha_2,	Hartman numbers;
k_1, k_2,	Debye-Hückel parameters;
$k_{\rm B}$,	Boltzmann constant;
$k_{\rm f_1}, k_{\rm f_2}$,	thermal conductivities of the fluid;
$k_{\rm f}$,	ratio of thermal conductivities of the fluid;
L,	length of the micro-channel;
$M_{\rm D}$,	dimensionless mass diffusion parameter;
n_0,	bulk ionic concentration;
$N_{\rm B1}, N_{\rm B2}$,	Brownian motion parameters;
$N_{\rm t1}, N_{\rm t2}$,	thermophoresis parameters;
Nu_1, Nu_2,	local Nusselt numbers;
$\overline{p}$,	pressure;
P_1, P_2,	non-dimensional pressure gradient parameters;
$q_{\rm w1}, q_{\rm w2}$,	wall heat fluxes on the two wall of the channel;
$R_{\rm D}$,	universal gas constant;
Re_1, Re_2,	Reynolds numbers;
s_1, s_2,	non-dimensional nano-particle volume fractions;
$S_{\rm e1}, S_{\rm e2}$,	strengths of lateral direction electric field;
$S_{\rm G}^1, S_{\rm G}^2$,	entropy generated in the respective channels;
$S_{\rm total}$,	total entropy generated in the channel;
$S_{\rm r}$,	ratio of entropy generated in Region I and Region II;
$\overline{T}_1, \overline{T}_2$,	temperatures;
T_0,	reference temperature;
$T_{\rm w}$,	temperature on the micro-channel wall surface;
$\widehat{T}$,	absolute temperature;
u_1, u_2,	non-dimensional velocities of the fluid;
$U_{\rm a1}, U_{\rm a2}$,	average velocities of the fluid;
$\overline{u}_1, \overline{u}_2$,	x-component of the fluid velocities;
W,	width of the micro-channel;
$\overline{x}, \overline{y}, \overline{z}$,	Cartesian coordinates;
$\widehat{z}$,	the valences of ions.

Greak letters

α_1, α_2,	thermal diffusivities of the nanofluid;
ε,	ratio of dielectric constants of the medium;
$\varepsilon_1, \varepsilon_2$,	dielectric constants of the medium;
ε_0,	permittivity of vacuum;
η,	non-dimensional spatial variable;
Γ_1, Γ_2,	non-dimensional pressure gradient parameters;
κ_1, κ_2,	electro-osmotic parameters;
Λ_0,	dimensionless reference nanoparticle parameter;
λ_N,	ratio of the respective quantity N such that $N \in \{\varepsilon, k_{\rm f}, \mu, \sigma, D_{\rm B}, D_{\rm t}, \alpha, \tau, \rho\}$;
μ_1, μ_2,	dynamic viscosities of the fluid;
θ_0,	dimensionless reference temperature parameter;
θ_1, θ_2,	non-dimensional temperature distributions;
$(\rho_1)_{\rm f}, (\rho_2)_{\rm s}$,	densities of the fluids or nanoparticles;
$\overline{\rho}_{\rm e1}, \overline{\rho}_{\rm e2}$,	charge densities;
$\tau_{\rm w1}, \tau_{\rm w2}$,	shear stresses on the wall of the micro-channel;
$\overline{\phi}_1, \overline{\phi}_2$,	electrostatic potentials;
ϕ_1, ϕ_2,	non-dimensional electrostatic potentials;
Ω_1, Ω_2,	ratios of Joule heating to the applied temperature differences between wall and ambient fluid;
ζ_1, ζ_2,	non-dimensional zeta potentials;
$\overline{\zeta}_1, \overline{\zeta}_2$,	zeta potentials.

Subscripts list

1, 2,	refer to quantities for Regions I and II;
f, s,	refer to the fluid and solid particles;
w,	physical quantities on the micro-channel wall.

1 Introduction

For evaluation of the precise characteristics of a fluid flow in a channel or a tube of micro-size, heat transfer has usually been a very important aspect to be considered. Flow transport

mechanism of microfluidics is of great importance in the design of all kinds of micro-electro-mechanical systems (MEMS) and has been investigated by some researchers[1–5]. In this context, heat dissipation is also a significant factor to be considered for better efficiency of those systems. That is to say, it is essential to develop efficient cooling systems that are compatible with the micro scale of these small structures. One appropriate way to achieve this target is the use of micro-channels or micro-tubes with high thermal conduction fluids passing through. However, a more effective way is the addition of small solid particles into the fluid for heat transfer enhancement. The latter approach was initiated by Maxwell[6] who utilized small metallic particles to increase the heat conductivity of regular fluids. Choi and Eastman[7] improved on heat transfer capability of fluids by adding nano-scale solid particles in the flow and named the resulting fluids as nanofluids. Using Choi's approach, the heat conductivity of the nanofluids is significantly improved and as a consequence, many different materials and their thermal properties, as well as other factors like shape and size were examined theoretically or experimentally by different researchers[8–15].

When a fluid flows due to external pressure, the static charge present in the solid channel walls attracts free-moving ions in the fluid and as a result, the electrical double layer (EDL)[16] on solid-fluid interface forms. In case of micro-channels and micro-tubes, the resistance is increased due to the reduced radius of the channel. In the meantime, a current is generated owing to the potential difference created from the rearrangement of these ions. This particular feature was studied by Mala et al.[17], Mala and Li[18], and Ren et al.[19]. Similar trends were highly observed in channels with tiny radius in many MEMS[20–23]. Ren and Li[24] proposed a symmetric boundary condition for the electrical field to explain the transportal process of EDL in a pressure driven system. Their work was followed by a study about the effects of EDL on the velocity distribution in a laminar flow by You and Guo[25]. Further investigations were done by Jing et al.[26], Srinivas[27], Qi and Ng[28], and Zheng and Jian[29], respectively. A good example of such flows is the electro-osmotic pumps, consisting of two layers in which fluids with different properties flow.

Many researchers have devoted themselves to studying convective heat transfer in a channel or tube; some illustrative works were done by Tao[30], Aung and Worku[31] and so on. However, rapid development of technology makes cooling system design more complicated. One layer heat transfer studies are inadequate to meet the present demands. In many industrial processes, multi-phase and multi-layer channels are expected to be used to replace single layer channels[32]. The two-layer fluids always generate a laminar fluid interface that behaves in a different way due to the boundary conditions on the dividing boundary of the channels. Owing to this particular behavior, those flows have vast applications in the fields related to bio-medical, bio-chemical, and biological analysis. The importance of biological sample separation apparatus could not be neglected in those applications. As a result, the fluid flowing through these micro-scale devices[33–34] has to be controlled and monitored precisely. In this context, some non-polar fluids are not completely driven by the electro-osmotic force. This was addressed by Brask et al.[35] who suggested high conductivity electrolyte solutions to increase the drag on the poorly conducting fluid. The electro-osmotic flow of two immiscible fluids was examined by Gao et al.[36], but the Maxwell stress balance condition was ignored at the interface. Shankar and Sharma[37] and Verma et al.[38] determined that a two-layer microfluid in the presence of electro-osmotic effects could not be correctly modeled without using the Maxwell stress balance condition. They used a Maxwell stress and shear stress balance condition on the interface between the two-layer microfluid flow which was verified by many further studies[39–41]. In particular, Xie and Jian[42] used this model to investigate an entropy analysis of a two-layer flow through micro-parallel channels under electro-osmotic effects. In their study, they used the model proposed in Refs. [37]–[38]. Zhao et al.[43] used a modified form of the Maxwell stress balance condition and demonstrated that in an immiscible two-layer flow, with EDL effects, the width of the EDL has a high influence on the flow but as the electro-osmotic parameters

increase to a sufficiently large value, i.e., smaller EDL thickness, there is no more influence from the EDL.

In order to preform a complete analysis, the entropy generation of the system needs to be considered as well. In a device with physical movement, there must be some irreversible losses of energy. In order to control and optimize these losses, this physical phenomenon has to be analyzed. Heat loss and generation is a major cause for these losses so that it is considered primarily in computation of the entropy generation of a system. This was first observed by Bejan[44]. A series of analyses for irreversibility energy losses through entropy generation function were discussed in Refs. [45]–[47]. Heat generation is a major factor but it is not the only factor responsible for the entropy generation. For example, Xu et al.[48] used six factors to compute the entropy of a system. Those factors are the irreversibility generated from heat transfer reversibility, Joule heating effect, viscous friction in the fluid, coupling electromagnetic diffusion, magnetic field and the nano-particle concentration. Xie and Jian[42] conducted the entropy generation analysis using the six mentioned factors for a two-layer flow.

This work aims to study a fully-developed steady immiscible two-layer flow in the presence of electro-kinetic effects due to EDL and an external electric field. These effects are accumulated in the momentum equations for the two layers. Buongiorno's model[49] is to be used to describe the nanoparticles and their behaviors in the fluid. The major difference between this work and the previous investigations[43,50–51] is that the balance of the Brownian diffusion and thermophoresis diffusion are considered in the boundary conditions at the fluid interface. Since the Brownian diffusion and thermophoresis diffusion are dominant factors for slip mechanisms of nanofluids, our model could be an appropriate one for description of two-layer flows of nanofluids. The solutions are obtained by transforming the governing partial differential equations into a set of ordinary differential equations by means of the HAM[52]. The focus is kept on the effects of physical parameters such as the Brinkman number Br, Hartman number Ha, the constant electric field parameter S_{e}, the electro-osmotic parameter κ, the thermophoresis parameter N_{t}, and the Brownian parameter N_{B} on the solutions themselves and the entropy generated in the system.

2 Mathematical modeling

We consider a steady, laminar, and fully developed flow of water based nanofluids in a two-layer micro-channel with effects of EDL in the presence of both external electric and magnetic fields. Figure 1 represents a three-dimensional (3D) physical sketch of the problem. The elongated rectangular micro-channel is placed horizontally with its width W sufficiently larger than its height H ($W/H > 4$, refer to Dauenhauer and Majdalani[53]). The length of the micro-channel L is assumed to be long enough to avoid the influence of the openings at the end. The heights of the lower and the upper layers are H_1 and H_2, respectively, satisfying $H_1 + H_2 = H$. With those assumptions, the interface of these two immiscible fluids is planar. Also, the parallel flow hypothesis can be applied so that the problem can be further reduced to a two-dimensional (2D) one. The simplified physical sketch is illustrated in Fig. 2, in which the Cartesian coordinate system $(\overline{x}, \overline{y}, \overline{z})$ is employed with $\overline{x}$ along the streamwise direction and $\overline{y}$ parallel

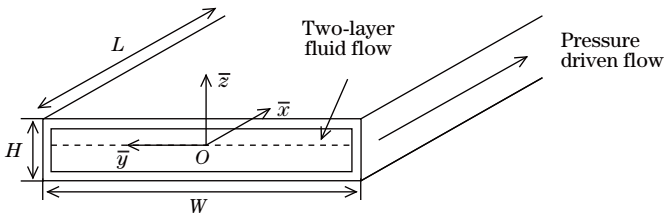

Fig. 1 3D physical sketch of the problem

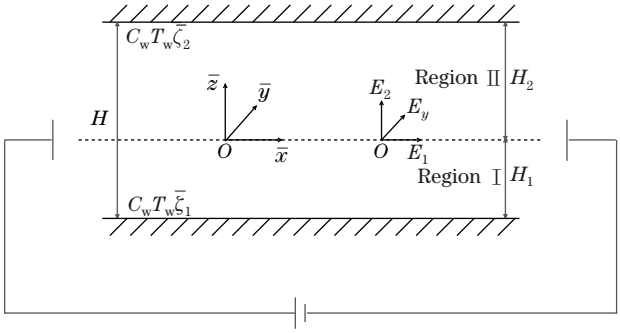

Fig. 2 2D physical sketch of the problem

to the surfaces and normal to $\overline{x}$, whereas $\overline{z}$ is perpendicular to the paralleled plates. Al_2O_3 nanoparticles are used in the lower channel, while TiO_2 nanoparticles are used in the upper channel. The physical properties of the fluid and the nanoparticles[54] are shown in Table 1. The zeta potentials, the temperature, and nanoparticle volumetric fractions on the lower and upper walls are $\overline{\zeta}_1, T_w, C_w$ and $\overline{\zeta}_2, T_w, C_w$, respectively. The external electric and magnetic fields are imposed on the system with E_x and E_y the electric fields in the direction of positive $\overline{x}$-axis and $\overline{y}$-axis, respectively, and B_0 the magnetic field normal to the channel walls in the direction of positive $\overline{z}$-axis.

Table 1 Physical properties of the fluid and nanoparticles

Physical property	Fluid (water)	Al_2O_3	TiO_2
$c_p/(\mathrm{J\cdot kg^{-1}\cdot K^{-1}})$	4 179.0	765.0	686.2
$\rho/(\mathrm{kg\cdot m^{-3}})$	997.1	3 970.0	4 250.0
$k/(\mathrm{W\cdot m^{-1}\cdot K^{-1}})$	0.613 0	40.000 0	8.953 8
$\alpha\times10^{-7}/(\mathrm{m^2\cdot s^{-1}})$	1.47	131.70	30.70
$\beta\times10^{-5}/(\mathrm{K^{-1}})$	21.00	0.85	0.90

It shall be noted that the EDL forms owing to the presence of static ions on the walls of the micro-channel. The ions form a diffuse layer which is not or less affected by the EDL. The ions present in the diffuse layer generate a current due to potential formed as a result of the redistribution of the ions. The fluid near this fixed layer has higher concentration of ions than ambient fluid. The electrostatic potential at any point is assumed to be satisfied by the Poisson equation.

The vector forms of the governing equations describing the distribution of the electric potential, total mass, momentum, energy, and nanoparticle volumetric fraction[42,49] are given as

$$\nabla^2\overline{\phi}_i = -\frac{\overline{\rho}_{ei}}{\varepsilon_0\,\varepsilon_i}, \tag{1}$$

$$\nabla\cdot V_i = 0, \tag{2}$$

$$\rho_i(V_i\cdot\nabla)V_i = -\nabla\overline{p} + \mu_i\nabla^2V_i + F_i, \tag{3}$$

$$\begin{aligned}&(\rho_ic_{pi})_{\mathrm{f}}(V_i\cdot\nabla)\overline{T_i}\\ &= k_{\mathrm{f}i}\nabla^2\overline{T}_i + (\rho_ic_{pi})_{\mathrm{s}}\Big(D_{\mathrm{B}i}\nabla\overline{T}_i\nabla\overline{C}_i + \Big(\frac{D_{\mathrm{t}i}}{T_0}\Big)\nabla\overline{T}_i\nabla\overline{T}_i\Big) + \frac{J_iJ_i}{\sigma_i} + \mu_i\overline{\Phi}_i,\end{aligned} \tag{4}$$

$$(V_i\cdot\nabla)\overline{C}_i = D_{\mathrm{B}i}\nabla^2\overline{C}_i + \Big(\frac{D_{\mathrm{t}i}}{T_0}\Big)\nabla^2\overline{T}_i, \tag{5}$$

where the subscript i $(i=1,2)$ denotes the lower and the upper fluid layers, respectively, $\overline{\phi}_i$ is the electric potential induced by EDL effects, $\overline{\rho}_{ei}$ is the charge density, ε_0 is the dielectric

constant, ε_i is the vacuum permittivity, V_i is the velocity vector, ρ_i is the density, c_{pi} is the specific heat and the subscripts "f" and "s" represent the quantities for fluid and solid particles, respectively. $\overline{p}$ is the pressure, μ_i is the viscosity, $F_i = \overline{\rho}_{ei}E + J_i \times B$ is the body force due to the electroosmosis and the electromagnetic forces in which E is the vector of the electric field, B is the imposed magnetic field, and $J_i = \sigma_i(E + V_i \times B)$ is the ion current density with σ_i the electrical conductivity, $\overline{T}_i$ is the fluid temperatures, $k_{\mathrm{f}i}$ is the thermal conductivity, $D_{\mathrm{B}i}$ is the Brownian diffusion coefficient, $\overline{C}_i$ is the nanoparticle volumetric fraction, $D_{\mathrm{t}i}$ is the thermophoretic diffusion coefficient, T_0 is the reference temperature, and $\overline{\Phi}_i$ is the viscous dissipation term, defined by

$$\begin{aligned}\overline{\Phi}_i =& 2\Big(\Big(\frac{\partial\overline{u}_i}{\partial\overline{x}}\Big)^2+\Big(\frac{\partial\overline{v}_i}{\partial\overline{y}}\Big)^2+\Big(\frac{\partial\overline{w}_i}{\partial\overline{z}}\Big)^2\Big)+\Big(\frac{\partial\overline{v}_i}{\partial\overline{x}}+\frac{\partial\overline{u}_i}{\partial\overline{y}}\Big)^2+\Big(\frac{\partial\overline{w}_i}{\partial\overline{y}}+\frac{\partial\overline{v}_i}{\partial\overline{z}}\Big)^2\\ &+\Big(\frac{\partial\overline{u}_i}{\partial\overline{z}}+\frac{\partial\overline{w}_i}{\partial\overline{x}}\Big)^2-\frac{2}{3}\Big(\frac{\partial\overline{u}_i}{\partial\overline{x}}+\frac{\partial\overline{v}_i}{\partial\overline{y}}+\frac{\partial\overline{w}_i}{\partial\overline{z}}\Big)^2,\end{aligned}\tag{6}$$

in which $\overline{u}_i$, $\overline{v}_i$, and $\overline{w}_i$ are velocity components in the $\overline{x}$-, $\overline{y}$-, and $\overline{z}$-directions, respectively.

Based on the parallel flow hypothesis, since the length of the micro-channel L is far greater than its height H, the flow velocity in the $\overline{z}$- direction is negligibly small, i.e., $\overline{w}_i \approx 0$. On the other hand, it has been known that the lateral electric field plays a more significant role than the magnetic field for the generation of the fluid motion, implying that $\overline{v}$ in the $\overline{y}$-direction can be neglected. As a result, only flow velocity along the $\overline{x}$-direction is taken into account. Hence, the continuity equation (2) is automatically satisfied. The Brownian diffusion term, the thermophoretic diffusion term, and the electromagnetic interaction term are considered in the energy equation. The former two terms are relevant in studying the flow in the micro-channels, while the fourth term is added to accumulate the Joule dissipation due to a magnetic field.

In light of the above assumptions, Eq. (2) is automatically satisfied, and Eq. (1) and Eqs. (3)–(5) are written as follows:

In Region I ($-H_1 \leqslant \overline{z} \leqslant 0$),

$$\frac{\partial^2\overline{\phi}_1}{\partial\overline{z}^2} = -\frac{\overline{\rho}_{\mathrm{e}1}(\overline{z})}{\varepsilon_0\varepsilon_1},\tag{7}$$

$$\mu_1\frac{\partial^2\overline{u}_1}{\partial\overline{z}^2}-\frac{\partial\overline{p}}{\partial\overline{x}}+E_x\overline{\rho}_{\mathrm{e}1}+\sigma_1B_0(E_y-B_0\overline{u}_1)=0,\tag{8}$$

$$\begin{aligned}\overline{u}_1\frac{\partial\overline{T}_1}{\partial\overline{x}}+\overline{w}_1\frac{\partial\overline{T}_1}{\partial\overline{z}} =& \alpha_1\frac{\partial^2\overline{T}_1}{\partial\overline{z}^2}+\tau_1\Big(D_{\mathrm{B}1}\frac{\partial\overline{T}_1}{\partial\overline{z}}\frac{\partial\overline{C}_1}{\partial\overline{z}}+\frac{D_{\mathrm{t}1}}{T_0}\Big(\frac{\partial\overline{T}_1}{\partial\overline{z}}\Big)^2\Big)\\ &+\frac{\sigma_1}{(\rho_1c_{p1})_{\mathrm{f}}}(E_x^2+E_y^2-2E_yB_0\overline{u}_1+B_0^2\overline{u}_1^2)+\frac{\mu_1}{(\rho_1c_{p1})_{\mathrm{f}}}\overline{\Phi}_1,\end{aligned}\tag{9}$$

$$\overline{u}_1\frac{\partial\overline{C}_1}{\partial\overline{x}}+\overline{w}_1\frac{\partial\overline{C}_1}{\partial\overline{z}}=D_{\mathrm{B}1}\frac{\partial^2\overline{C}_1}{\partial\overline{z}^2}+\frac{D_{\mathrm{t}1}}{T_0}\frac{\partial^2\overline{T}_1}{\partial\overline{z}^2}.\tag{10}$$

In Region II ($0 \leqslant \eta \leqslant H_2$),

$$\frac{\partial^2\overline{\phi}_2}{\partial\overline{z}^2} = -\frac{\overline{\rho}_{\mathrm{e}2}(\overline{z})}{\varepsilon_0\varepsilon_2},\tag{11}$$

$$\mu_2\frac{\partial^2\overline{u}_2}{\partial\overline{z}^2}-\frac{\partial\overline{p}}{\partial\overline{x}}+E_x\overline{\rho}_{\mathrm{e}2}+\sigma_2B_0(E_y-B_0\overline{u}_2)=0,\tag{12}$$

$$\overline{u}_2\frac{\partial\overline{T}_2}{\partial\overline{x}}+\overline{w}_2\frac{\partial\overline{T}_2}{\partial\overline{z}}=\alpha_2\frac{\partial^2\overline{T}_2}{\partial\overline{z}^2}+\tau_2\Big(D_{\mathrm{B}2}\frac{\partial\overline{T}_2}{\partial\overline{z}}\frac{\partial\overline{C}_2}{\partial\overline{z}}+\frac{D_{\mathrm{t}2}}{T_0}\Big(\frac{\partial\overline{T}_2}{\partial\overline{z}}\Big)^2\Big)$$
$$+\frac{\sigma_2}{(\rho_2c_{p2})_{\mathrm{f}}}(E_x^2+E_y^2-2E_yB_0\overline{u}_2+B_0^2\overline{u}_2^2)+\frac{\mu_2}{(\rho_2c_{p2})_{\mathrm{f}}}\overline{\Phi}_2, \tag{13}$$

$$\overline{u}_2\frac{\partial\overline{C}_2}{\partial\overline{x}}+\overline{w}_2\frac{\partial\overline{C}_2}{\partial\overline{z}}=D_{\mathrm{B}2}\frac{\partial^2\overline{C}_2}{\partial\overline{z}^2}+\frac{D_{\mathrm{t}2}}{T_0}\frac{\partial^2\overline{T}_2}{\partial\overline{z}^2}. \tag{14}$$

Here, E_x and E_y are the strength of the electrical fields along the $\overline{x}$- and $\overline{y}$-directions, respectively, B_0 is the strength of the magnetic field along the z-direction, $\alpha_i=k_{\mathrm{f}i}/(\rho_ic_{pi})_{\mathrm{f}}$ is the thermal diffusivity, and $\tau_i=(\rho_ic_{pi})_{\mathrm{s}}/(\rho_ic_{pi})_{\mathrm{f}}$ is the heat capacity ratio with $i=1,2$ representing the lower and upper fluid layers. The values for $(\rho_ic_{pi})_{\mathrm{f}}$, $(\rho_ic_{pi})_{\mathrm{s}}$, $k_{\mathrm{f}i}$, and α_i are given in Table 1.

The electric potentials, flow velocities, temperatures, nano-particle volumetric concentrations, and flux are assumed to be continuous at the interface. Velocities on the boundaries satisfy the no-slip condition, and the temperature and nano-particle concentration on the boundaries are constant distributions. Hence, the boundary conditions for Eqs. (8)–(14) are given as

$$\begin{cases}\overline{z}=-H_1\colon & \overline{\phi}_1=\overline{\zeta}_1,\quad \overline{u}_1=0,\quad \overline{T}_1=T_{\mathrm{w}},\quad \overline{C}_1=C_{\mathrm{w}},\\ \overline{z}=0\colon & \begin{cases}\overline{\phi}_1=\overline{\phi}_2,\quad \overline{u}_1=\overline{u}_2,\quad \overline{T}_1=\overline{T}_2,\quad \overline{C}_1=\overline{C}_2,\\ \varepsilon_1\dfrac{\partial\overline{\phi}_1}{\partial\overline{z}}=\varepsilon_2\dfrac{\partial\overline{\phi}_2}{\partial\overline{z}},\quad \mu_1\dfrac{\partial\overline{u}_1}{\partial\overline{z}}=\mu_2\dfrac{\partial\overline{u}_2}{\partial\overline{z}},\quad k_{\mathrm{f}_1}\dfrac{\partial\overline{T}_1}{\partial\overline{z}}=k_{\mathrm{f}_2}\dfrac{\partial\overline{T}_2}{\partial\overline{z}},\\ \dfrac{D_{\mathrm{t}1}}{T_0}\dfrac{\partial\overline{T}_1}{\partial\overline{z}}+D_{\mathrm{B}1}\dfrac{\partial\overline{C}_1}{\partial\overline{z}}=\dfrac{D_{\mathrm{t}2}}{T_0}\dfrac{\partial\overline{T}_2}{\partial\overline{z}}+D_{\mathrm{B}2}\dfrac{\partial\overline{C}_2}{\partial\overline{z}},\end{cases}\\ \overline{z}=H_2\colon & \overline{\phi}_2=\overline{\zeta}_2,\quad \overline{u}_2=0,\quad \overline{T}_2=T_{\mathrm{w}},\quad \overline{C}_2=C_{\mathrm{w}}.\end{cases} \tag{15}$$

When the dielectric constant is assumed to be uniform, the equilibrium Boltzmann distribution can be given by

$$\rho_{\mathrm{e}i}=-2n_0\widehat{z}e\sinh\Big(\frac{\widehat{z}e\overline{\phi}_i(\overline{z})}{k_{\mathrm{B}}\widehat{T}}\Big),\quad i=1,2, \tag{16}$$

where n_0, $\widehat{z}$, e, k_{B}, and $\widehat{T}$ are, respectively, the bulk ionic concentration, the valence of ions, the fundamental charge, the Boltzmann constant, and the absolute temperature. In this way, the Poisson-Boltzmann equation is simplified to (see Ref. [43])

$$\frac{\partial^2\overline{\phi}_i}{\partial\overline{z}^2}=\frac{2n_0\widehat{z}e}{\varepsilon_0\varepsilon_i}\sinh\Big(\frac{\widehat{z}e\overline{\phi}_i(\overline{z})}{k_{\mathrm{B}}\widehat{T}}\Big),\quad i=1,2. \tag{17}$$

If the electrical potential is significantly smaller than the thermal energy of the ions, i.e., $|k_{\mathrm{B}}\widehat{T}|\ll|z_ie\overline{\phi}_i(z)|$, the Debye-Hückel linear approximation can be used, hence Eq. (17) is reduced to

$$\frac{\partial^2\overline{\phi}_i}{\partial\overline{z}^2}-\Big(\frac{2n_0\widehat{z}^2e^2}{\varepsilon_0\varepsilon_ik_{\mathrm{B}}\widehat{T}}\Big)\overline{\phi}_i=0,\quad i=1,2. \tag{18}$$

3 Non-dimensional reduction

To eliminate the dimensional influence, we define the following similarity variables:

$$\eta=\frac{\overline{z}}{H},\quad \phi_i=\frac{\widehat{z}e\overline{\phi}_i}{k_{\mathrm{B}}\widehat{T}},\quad u_i=\frac{\overline{u}_i}{U_{\mathrm{a}i}},\quad \theta_i=\frac{\overline{T}_i-T_0}{T_{\mathrm{w}}-T_0},\quad s_i=\frac{\overline{C}_i-C_0}{C_{\mathrm{w}}-C_0}. \tag{19}$$

Note that after utility of the above-mentioned similarity transformations, the fluid flow region is changed to $[-h_1,h_2]$ with $h_1=H_1/H$ and $h_2=H_2/H$.

Substituting Eq. (19) into the set of governing equations (7)–(14) and (18), we obtain the following equations.

In Region I ($-h_1 \leqslant \eta \leqslant 0$),

$$\phi_1'' - \kappa_1^2 \phi_1 = 0, \tag{20}$$

$$u_1'' - Ha_1^2 u_1 + S_{\mathrm{e}1} Ha_1 + \Gamma_1 + \kappa_1^2 \phi_1 = 0, \tag{21}$$

$$\theta_1'' + N_{\mathrm{B}1}\theta_1' s_1' + N_{\mathrm{t}1}\theta_1'^2 + Br_1(u_1'^2 + Ha_1^2 u_1^2 - 2S_{\mathrm{e}1} Ha_1 u_1) + \Omega_1 = 0, \tag{22}$$

$$s_1'' + \frac{N_{\mathrm{t}1}}{N_{\mathrm{B}1}}\theta_1'' = 0. \tag{23}$$

In Region II ($0 \leqslant \eta \leqslant h_2$),

$$\phi_2'' - \kappa_2^2 \phi_2 = 0, \tag{24}$$

$$u_2'' - Ha_2^2 u_2 + S_{\mathrm{e}2} Ha_2 + \Gamma_2 + \kappa_2^2 \phi_2 = 0, \tag{25}$$

$$\theta_2'' + N_{\mathrm{B}2}\theta_2' s_2' + N_{\mathrm{t}2}\theta_2'^2 + Br_2(u_2'^2 + Ha_2^2 u_2^2 - 2S_{\mathrm{e}2} Ha_2 u_2) + \Omega_2 = 0, \tag{26}$$

$$s_2'' + \frac{N_{\mathrm{t}2}}{N_{\mathrm{B}2}}\theta_2'' = 0. \tag{27}$$

Correspondingly, their boundary conditions are reduced to

$$\begin{cases} \eta = -h_1: & \phi_1 = \zeta_1, \quad u_1 = 0, \quad \theta_1 = 1, \quad s_1 = 1, \\ \eta = 0: & \begin{cases} \phi_1 = \phi_2 \quad \phi_1' = \lambda_\varepsilon \phi_2', \quad u_1 = \dfrac{\lambda_\varepsilon}{\lambda_\mu} u_2, \quad u_1' = \lambda_\varepsilon u_2', \\ \theta_1 = \theta_2, \quad s_1 = s_2, \quad \theta_1' = \lambda_{k_{\mathrm{f}}} \theta_2', \\ N_{\mathrm{B}1}(s_1' - \lambda_{D_{\mathrm{B}}} s_2') + N_{\mathrm{t}1}(\theta_1' - \lambda_{D_{\mathrm{t}}} \theta_2') = 0, \end{cases} \\ \eta = h_2: & \phi_2 = \zeta_2, \quad u_2 = 0, \quad \theta_2 = 1, \quad s_2 = 1, \end{cases} \tag{28}$$

where $\zeta_i = \widehat{z} e_0 \overline{\zeta}_i / (k_{\mathrm{B}} \widehat{T})$ is the zeta potential, and κ_i, Ha_i, $S_{\mathrm{e}i}$, Γ_i, $U_{\mathrm{a}i}$, $N_{\mathrm{B}i}$, $N_{\mathrm{t}i}$, Br_i, and Ω_i are, respectively, the electro-osmotic parameters, the Hartman numbers, the electric field parameters, the constant pressure gradient parameters, the electro-osmotic velocity, the Brownian motion parameters, the thermophoresis parameters, the Brinkman numbers, and ratio of Joule heating to the applied temperature difference between the wall and the ambient fluid, which are defined as follows:

$$\kappa_i = \widehat{z} e H \sqrt{\frac{2n_0}{\varepsilon_0 \varepsilon_i k_{\mathrm{B}} \widehat{T}}}, \quad Ha_i = B_0 H \sqrt{\frac{\sigma_i}{\mu_i}}, \quad S_{\mathrm{e}i} = \frac{E_y H}{U_{\mathrm{a}i}} \sqrt{\frac{\sigma_i}{\mu_i}},$$

$$\Gamma_i = -\frac{H^2}{\mu_i U_{\mathrm{a}i}} \frac{\mathrm{d}\overline{p}}{\mathrm{d}\overline{x}}, \quad U_{\mathrm{a}i} = \frac{\varepsilon_i E_x k_{\mathrm{B}} \widehat{T}}{\mu_i \widehat{z} e}, \quad N_{\mathrm{B}i} = \frac{\tau_i D_{\mathrm{B}i}(C_{\mathrm{w}} - C_0)}{\alpha_i},$$

$$N_{\mathrm{t}i} = \frac{\tau_i (T_{\mathrm{w}} - T_0)}{\alpha_i} \Big(\frac{D_{\mathrm{t}i}}{T_0} \Big), \quad Br_i = \frac{\mu_i U_{\mathrm{a}i}^2}{k_{\mathrm{f}i}(T_{\mathrm{w}} - T_0)}, \quad \Omega_i = \frac{\sigma_i (E_x^2 + E_y^2) H^2}{k_{\mathrm{f}_i}(T_{\mathrm{w}} - T_0)}.$$

To measure the difference of physical properties of two layer nanofluids, the following ratios are defined:

$$\lambda_\varepsilon = \frac{\varepsilon_2}{\varepsilon_1}, \quad \lambda_{k_{\mathrm{f}}} = \frac{k_{\mathrm{f}_2}}{k_{\mathrm{f}_1}}, \quad \lambda_\mu = \frac{\mu_2}{\mu_1}, \quad \lambda_\sigma = \frac{\sigma_2}{\sigma_1},$$

$$\lambda_{D_{\mathrm{B}}} = \frac{D_{\mathrm{B}2}}{D_{\mathrm{B}1}}, \quad \lambda_{D_{\mathrm{t}}} = \frac{D_{\mathrm{t}2}}{D_{\mathrm{t}1}}, \quad \lambda_\alpha = \frac{\alpha_2}{\alpha_1}, \quad \lambda_\tau = \frac{\tau_2}{\tau_1},$$

which give the connections between two-layer physical parameters as follows:

$$
\begin{aligned}
&U_{\mathrm{a}2}=\frac{\lambda_\varepsilon}{\lambda_\mu}U_{\mathrm{a}1},\quad Ha_2=\sqrt{\frac{\lambda_\sigma}{\lambda_\mu}}Ha_1,\quad S_{\mathrm{e}2}=\frac{\sqrt{\lambda_\mu\lambda_\sigma}}{\lambda_\varepsilon}S_{\mathrm{e}1},\\
&Br_2=\frac{\lambda_\varepsilon^2}{\lambda_{k_{\mathrm{f}}}\lambda_\mu}Br_1,\quad \Gamma_2=\frac{1}{\lambda_\varepsilon}\Gamma_1,\quad \kappa_2=\frac{1}{\sqrt{\lambda_\varepsilon}}\kappa_1,\quad \Omega_2=\frac{\lambda_\sigma}{\lambda_{k_{\mathrm{f}}}}\Omega_1,\\
&N_{\mathrm{B}2}=\frac{\lambda_\tau\lambda_{D_{\mathrm{B}}}}{\lambda_\alpha}N_{\mathrm{B}1},\quad N_{\mathrm{t}2}=\frac{\lambda_\tau\lambda_{D_{\mathrm{t}}}}{\lambda_\alpha}N_{\mathrm{t}1}.
\end{aligned}
$$

In this analysis, some ratios are chosen based on Table 1 as $\lambda_{k_{\mathrm{f}}}=1$, $\lambda_\mu=1$, $\lambda_\alpha=1$, and $\lambda_\tau=0.96$, and other ratios are chosen as $\lambda_\sigma=1.2$, $\lambda_\varepsilon=1.2$, $\lambda_{D_{\mathrm{B}}}=1.2$, $\lambda_{D_{\mathrm{t}}}=1.2$, and $\lambda_\rho=1$.

4 Entropy analysis and other physical quantities

Since the two-layer velocity, temperature and nano-particle concentration distributions can be determined by solving Eqs. (20)–(23) and Eqs. (24)–(27), the entropy generation distribution through the two-layer micro-channel can be computed correspondingly. The rate of two-layer fluid entropy generation S^i_{GG} is given as[45]

$$
S^i_{\mathrm{GG}}=S^i_{\mathrm{GH}}+S^i_{\mathrm{GJ}}+S^i_{\mathrm{GF}}+S^i_{\mathrm{GE}}+S^i_{\mathrm{GM}}+S^i_{\mathrm{GC}},\tag{29}
$$

where S^i_{GH}, S^i_{GJ}, S^i_{GF}, S^i_{GE}, S^i_{GM}, and S^i_{GC} represent the local volumetric entropy generation rate due to heat transfer reversibility, Joule heating effect, viscous friction in the fluid, coupling electromagnetic diffusion, magnetic field and the nanoparticle concentration, respectively, which are defined as

$$
\begin{cases}
S^i_{\mathrm{GH}}=\dfrac{k_{\mathrm{f}i}}{\overline{T}_i^2}\Big(\dfrac{\partial\overline{T}_i}{\partial\overline{z}}\Big)^2,\quad S^i_{\mathrm{GJ}}=\dfrac{\sigma_i(E_x^2+E_y^2)}{\overline{T}_i},\quad S^i_{\mathrm{GF}}=\dfrac{\mu_i}{\overline{T}_i}\Big(\dfrac{\partial\overline{u}_i}{\partial\overline{z}}\Big)^2,\\
S^i_{\mathrm{GE}}=\dfrac{\sigma_i(2E_yB_0\overline{u}_i)}{\overline{T}_i},\quad S^i_{\mathrm{GM}}=\dfrac{\sigma_i(B_0\overline{u}_i^2)}{\overline{T}_i},\quad S^i_{\mathrm{GC}}=\dfrac{R_{\mathrm{D}}}{\overline{C}_i}\Big(\dfrac{\partial\overline{C}_i}{\partial\overline{z}}\Big)^2+\dfrac{R_{\mathrm{D}}}{\overline{T}_i}\dfrac{\partial\overline{C}_i}{\partial\overline{z}}\dfrac{\partial\overline{T}_i}{\partial\overline{z}},
\end{cases}\tag{30}
$$

where R_{D} is the universal gas constant, and $i=1,2$ represent layer I and layer II, respectively.

The non-dimensional form of Eq. (29) can be obtained by using variables (19) in the above definitions. Therefore, the characteristic entropy transfer rate, $S^i_{\mathrm{G}}=h^2S^i_{\mathrm{GG}}/k_{\mathrm{f}_1}$, for the ith layer is given by

$$
\begin{aligned}
S^1_{\mathrm{G}}=&\frac{1}{\theta_1+\theta_0}\Big(\frac{1}{\theta_1+\theta_0}\theta_1'^2+\Omega_1+Br_1u_1'^2+2Ha_1S_{\mathrm{e}1}Br_1u_1+Ha_1^2Br_1u_1^2\Big)\\
&+\frac{M_{\mathrm{D}}}{s_1+\Lambda_0}s_1'^2+\frac{M_{\mathrm{D}}}{\theta_1+\theta_0}s_1'\theta_1',
\end{aligned}\tag{31}
$$

$$
\begin{aligned}
S^2_{\mathrm{G}}=&\frac{\lambda_{k_{\mathrm{f}}}}{\theta_2+\theta_0}\Big(\frac{1}{\theta_2+\theta_0}\theta_2'^2+\Omega_2+Br_2u_2'^2+2Ha_2S_{\mathrm{e}2}Br_2u_2+Ha_2^2Br_2u_2^2\Big)\\
&+\frac{M_{\mathrm{D}}}{s_2+\Lambda_0}s_2'^2+\frac{M_{\mathrm{D}}}{\theta_2+\theta_0}s_2'\theta_2',
\end{aligned}\tag{32}
$$

where M_{D}, θ_0, and Λ_0 are, respectively, the dimensionless mass diffusion parameter, the reference temperature to wall-ambient temperature difference ratio, and the reference nanoparticle volume fraction to the wall-ambient nanoparticle volume fraction difference ratio, which are given as

$$
M_{\mathrm{D}}=\frac{R_{\mathrm{D}}(C_{\mathrm{w}}-C_0)}{k_{\mathrm{f}_1}},\quad \theta_0=\frac{T_0}{T_{\mathrm{w}}-T_0},\quad \Lambda_0=\frac{C_0}{C_{\mathrm{w}}-C_0}.
$$

In this way, the total entropy generated in the two layers is given as

$$S_{\text{total}} = \int_{-h_1}^{0} S_{\text{G}}^{1} \mathrm{d}\eta + \int_{0}^{h_2} S_{\text{G}}^{2} \mathrm{d}\eta. \tag{33}$$

The physical quantities of practical interest for this problem are the skin friction coefficient and the Nusselt number, which are defined by

$$C_{\text{f}i} = \frac{\tau_{\text{w}_i}}{\dfrac{1}{2}\rho_i U_{\text{a}i}^2}, \quad Nu_i = \frac{H_i q_{\text{w}_i}}{k_{\text{f}i}(T_{\text{w}} - T_0)}, \tag{34}$$

where i $(i = 1, 2)$ represents the respective layer, τ_{w_i} is the shear stress, and q_{w_i} is the heat flux on the walls, which are given by

$$\tau_{\text{w}_i} = \mu_i \frac{\partial \overline{u}_i}{\partial \overline{z}}\Big|_{\overline{z}=(-1)^i H_i}, \quad q_{\text{w}_i} = -k_{\text{f}i} \frac{\partial \overline{T}_i}{\partial \overline{z}}\Big|_{\overline{z}=(-1)^i H_i}. \tag{35}$$

Substituting Eqs. (19) and (35) into Eq. (34), we obtain

$$C_{\text{f}i} = \frac{2}{Re_i} u_i'((-1)^i h_i), \quad Nu_i = -\frac{h_i}{H} \theta_i'((-1)^i h_i), \tag{36}$$

where Re_i is the Reynolds number, defined by

$$Re_i = \frac{H \rho_i U_{\text{a}i}}{\mu_i}.$$

The relation of the Reynolds number between two layers is

$$Re_2 = \frac{\lambda_\rho \lambda_\varepsilon}{\lambda_\mu^2} Re_1,$$

where $\lambda_\rho = \rho_2/\rho_1$,

5 Results and discussion

The HAM[52] is used to obtain the accurate solutions for the system of equations (20)–(27). The solution process is listed in Appendix A. The precision of those solutions is checked using the error evaluation function, which is defined, based on the maximum total average squared error, by

$$E(m) = \max\{E_{\phi_i}(m), E_{u_i}(m), E_{\theta_i}(m), E_{s_i}(m) | i = 1, 2\}, \tag{37}$$

where m is the HAM computational order, and $E_{\phi_i}(m), E_{u_i}(m), E_{\theta_i}(m), E_{s_i}(m)$ are error evaluation functions defined based on Eqs. (20)–(27) and are listed in Appendix B.

The mth order error is obtained by substituting the corresponding solutions into Eq. (37). When all HAM auxiliary parameters and physical parameters are properly given, the errors are computed, as shown in Table 2. It is found from the table that the error decreases rapidly as the computational order of HAM increases, which guarantees the solutions' convergence. The range for the Hartman number is from 1 to 10[55]. This range can vary and depend on the values of other parameters, such as the Brinkman number. In this study, the Brinkman number is varied between 0 and 1 to keep the system stable. For the assumption of a unidirectional flow, the value of the non-dimensional electric field parameter $S_{\text{e}1}$ cannot be considered too large[56]. Hence, it is kept at 1 for all the analyses. The value for this parameter is varied

and is mentioned accordingly when special statements are made or a trend is observed for this parameter. Similarly, the value for the thermophoretic diffusion parameter is kept low, in the range of 0 to 1. Other parameters are chosen as $\zeta_1 = \zeta_2 = 1$, $H_1 = 1$, $H_2 = 2$, $\Omega_1 = 1$ and $N_{t1} = N_{B1} = 0.1$. Note also that the Homotopy-Padé technique[52] is used to improve the precision, which indicates that the convergence control parameters are insignificant and can be prescribed to any fixed nonzero value.

Table 2 The maximum error $E(m)$

Order	$\kappa_1 = 1$	$\kappa_1 = 3$	$\kappa_1 = 5$	$\kappa_1 = 10$
10	19.864	20.850	5 883.7	8 257.1
20	2.74×10^{-4}	3.02×10^{-4}	1.8×10^{-4}	0.014
30	2.92×10^{-9}	2.09×10^{-9}	2.32×10^{-10}	1.37×10^{-4}
40	8.96×10^{-14}	7.46×10^{-14}	1.78×10^{-15}	5.51×10^{-6}
50	7.05×10^{-18}	1.04×10^{-17}	1.26×10^{-20}	5.023×10^{-15}

We then discuss the effect of various parameters on different physical fields. It is known that the governing equations (20) and (24) admit analytical solutions of the form,

$$\phi_1(\eta) = C_1 \cosh(\kappa_1 \eta) + C_2 \sinh(\kappa_1 \eta), \tag{38}$$

$$\phi_2(\eta) = C_1 \cosh(\kappa_2 \eta) + \frac{\kappa_1}{\lambda_\varepsilon \kappa_2} C_2 \sinh(\kappa_2 \eta), \tag{39}$$

where

$$C_1 = \frac{\lambda_\varepsilon \kappa_2 \zeta_2 \sinh(h_1 \kappa_1) - \kappa_1 \zeta_1 \sinh(h_2 \kappa_2)}{\lambda_\varepsilon \kappa_2 \cosh(h_2 \kappa_2) \sinh(h_1 \kappa_1) + \kappa_1 \cosh(h_1 \kappa_1) \sinh(h_2 \kappa_2)}, \tag{40}$$

$$C_2 = \frac{\lambda_\varepsilon \kappa_2 (\kappa_1 \zeta_2 \cosh(h_1 \kappa_1) - \kappa_1 \zeta_1 \cosh(h_2 \kappa_2))}{\kappa_1 (\lambda_\varepsilon \kappa_2 \cosh(h_2 \kappa_2) \sinh(h_1 \kappa_1) + \kappa_1 \cosh(h_1 \kappa_1) \sinh(h_2 \kappa_2))}. \tag{41}$$

These analytical solutions can be used to verify the accuracy of the HAM results. As shown in Fig. 3, solutions given by two different approaches match each other in the whole domain. This again confirms the validity of the proposed technique. It is seen that the electrical potential $\phi(\eta)$ decreases monotonously as the electro-osmotic parameter κ_1 enlarges. Physically, the increase in κ_i indicates the increase in the height of the channel, and the effect of the EDL on the inner part of the channel is therefore weakened. We then consider the influence of the ratio of the electro-osmotic parameter λ_ε on the electrical potential $\phi(\eta)$. As shown, the electrostatic potential field reduces as the dielectric ratio λ_ε grows. Note that the smaller value of λ_ε implies a thinner EDL on the upper wall as compared with the lower wall. Figure 4 presents the variation of the velocity profile $u(\eta)$ with the electro-osmotic parameter κ_1. It is seen from the figure that the increase in κ_1 causes an enhancement of the velocity profile. This is due to the electrical force due to the joint effects of the external electric field and magnetic field has an opposite direction to the fluid motion caused by the pressure, so the resistance due to the EDL becomes smaller and smaller as κ_1 continuously grows.

It is known that viscosity has distinct influence in the boundary layer region in the vicinity of the channel walls. When the channel is thin enough, this effect could affect the whole channel flow, especially for the temperature distribution. It is known that the Brinkman number represents the ratio of viscous heat generation to external heating and plays an important role in the temperature distribution. Therefore, it is essential to investigate its influence on temperature profile. Figure 5 shows the variation in the temperature distribution $\theta(\eta)$ with evolution in Br_1. It can be seen that as Br_i increases, the temperature increases near both walls of the channel but drops in the middle part. This implies higher viscous dissipation near the channel walls and higher molecular conduction in the middle part of the channel with an increase in the Brinkman number.

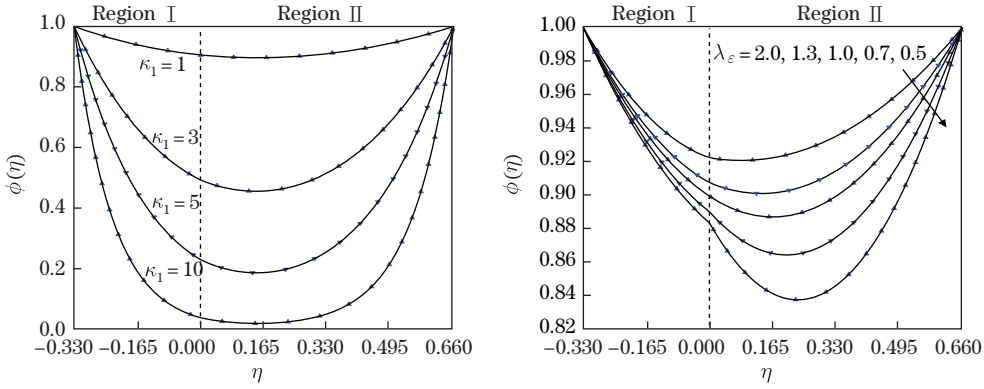

Fig. 3 Comparison of the solutions for $\phi(\eta)$ obtained by different approaches with variation in the electro-osmotic properties of the flow. Line: HAM results, symbols: analytical solutions given by Eqs. (38) and (39) in the case of $\zeta_1 = \zeta_2 = 1$, $H_1 = 1$, $H_2 = 2$, $Ha_1 = S_{e1} = \Omega_1 = 1$, $Br_1 = 0.1$, and $N_{t1} = N_{B1} = 0.1$ and κ_1=1 for the right side

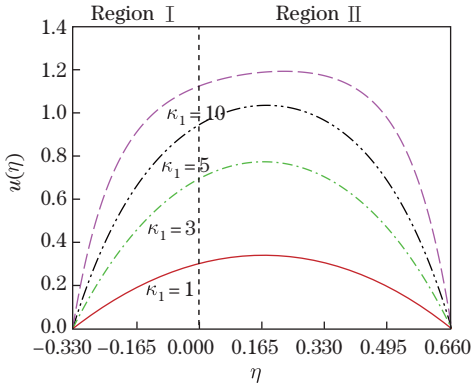

Fig. 4 The velocity profile $u(\eta)$ against η for various values of the electro-osmotic parameter κ_1 in the case of $\zeta_1 = \zeta_2 = 1$, $H_1 = 1$, $H_2 = 2$, $Ha_1 = S_{e1} = \Omega_1 = 1$, $Br_1 = 0.1$, and $N_{t1} = N_{B1} = 0.1$

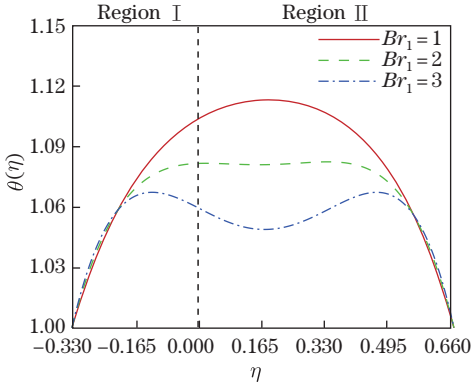

Fig. 5 The temperature profile $\theta(\eta)$ against η for various values of the Brinkman number Br_1 in the case of $\zeta_1 = \zeta_2 = 1$, $H_1 = 1$, $H_2 = 2$, $Ha_1 = S_{e1} = \Omega_1 = \kappa_1 = 1$, and $N_{t1} = N_{B1} = 0.1$

Figure 6 illustrates the change in temperature distribution $\theta(\eta)$ due to variation in the thermophoresis diffusion ratio λ_{D_t}. It is found that the maximum amplitude of the temperature

shifts towards the upper channel wall as λ_{D_t} increases. Simultaneously, the temperature profile decreases near the lower wall but increases near the upper wall. This is because the increase in the thermophoresis diffusion coefficient in the upper channel results in an increase in the acceleration of the particles in the region. Heat transfer is therefore enhanced accordingly. Figure 7 depicts the variation of nanoparticle volume fraction profile $s(\eta)$ with the increase in the thermophoresis parameter N_{t1} and the thermophoresis diffusion ratio λ_{D_t}. It is known that there is a temperature difference between the channel walls and the inner fluid, which results in the thermophoresis diffusion represented by N_{ti}. As shown in the figure, the nanoparticle volume fraction decreases rapidly as N_{ti} increases. This shows that the thermophoresis diffusion variation is highly important for the distribution of nanoparticles. Similarly, the fluid thermal properties could affect the distribution of nanoparticles as well. It is observed that an increase in λ_{D_t} speeds up the movement of nanoparticles towards the upper wall. As a result, the nanoparticle volume fraction decreases accordingly.

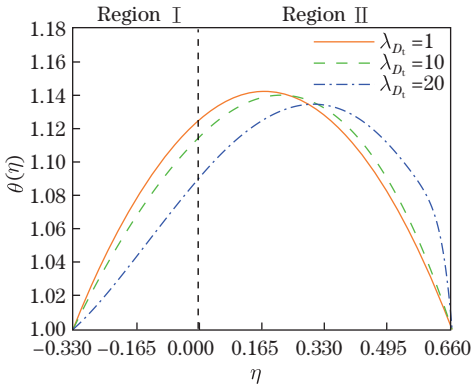

Fig. 6 The temperature profile $\theta(\eta)$ against η for various values of the thermophoresis diffusion ratio λ_{D_t} in the case of $\zeta_1 = \zeta_2 = 1$, $H_1 = 1$, $H_2 = 2$, $Ha_1 = S_{e1} = \Omega_1 = \kappa_1 = 1$, $Br_1 = 0.1$ and $N_{t1} = N_{B1} = 0.1$ (color online)

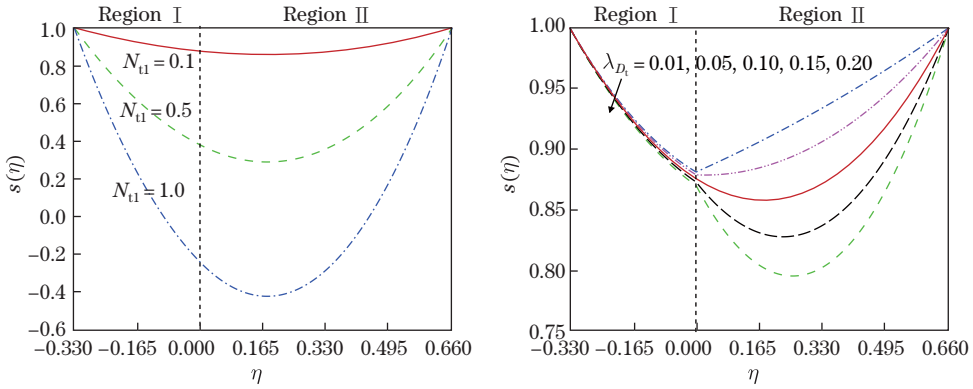

Fig. 7 The nanoparticle volume fraction profile $s(\eta)$ against η for some thermophoresis diffusion related parameters in the case of $\zeta_1 = \zeta_2 = 1$, $H_1 = 1$, $H_2 = 2$, $Ha_1 = S_{e1} = \Omega_1 = \kappa_1 = 1$, $Br_1 = 0.1$, $N_{B1} = 0.1$, and N_{t1}=0.1 for the right side (color online)

The impacts of physical ratios on the flow characteristics are illustrated in Figs. 8 and 9. Here, the trends for velocity and temperature fields are observed with respect to change in the ratios for viscosity, electrical conductivity and thermal conductivity. It can be seen in Fig. 8 that with increase in the viscosity ratio λ_μ, the peak flow velocity shifts towards Region I and

the flow velocity decreases throughout the channel. This is due to the fact that the average velocity in Region II depends on this ratio and with increase in λ_μ, there is a decrease in Region II average velocity. Physically, this means that for a higher value of λ_μ, the viscosity in Region II is greater as compared with Region I and hence, a decrease in Region II velocity is observed. On the other hand, the flow velocity increases throughout the channel with increase in λ_ε. This is due to the fact that the average velocity in Region II is directly proportional to this ratio. Physically, it implies that due to increase in the electrical conductivity in Region II, the flow velocity in this part of the channel increases and as a result the velocity in the whole channel increases.

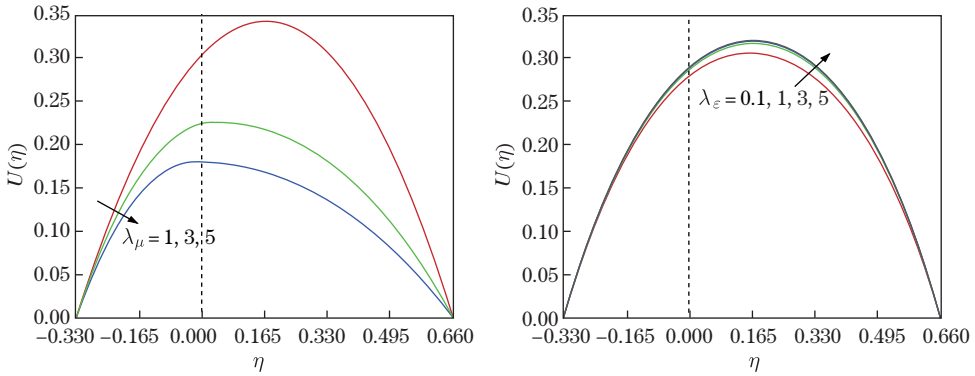

Fig. 8 Variation in velocity with change in the physical ratios λ_μ and λ_ε in case of $\zeta_1 = \zeta_2 = 1$, $H_1 = 1$, $H_2 = 2$, $Ha_1 = 3$, $S_{e1} = \Omega_1 = 1$, $Br_1 = 0.1$, and $N_{t1} = N_{B1} = 1$ (color online)

A similar analysis is carried out for the temperature field in Fig. 9, where the trend in the temperature field is observed with respect to the viscosity and thermal conductivity ratios. It can be seen that with the increase in the viscosity ratio λ_μ, there is a slight increase in the temperature field throughout the domain. This is due to the fact that the temperature increases as the viscous force increases in the channel. With an increase in λ_μ, an increase in Region II viscosity is anticipated which results in an increase in the temperature of the flow. Finally, the temperature field with variation in the thermal conductivity ratio is observed. It can be seen that the temperature throughout the channel decreases as λ_{k_f} increases. This is due to the fact that as λ_{k_f} increases, the molecular conduction in Region II increases. This results in a decrease in Region II temperature and as a consequence, the temperature throughout the channel drops.

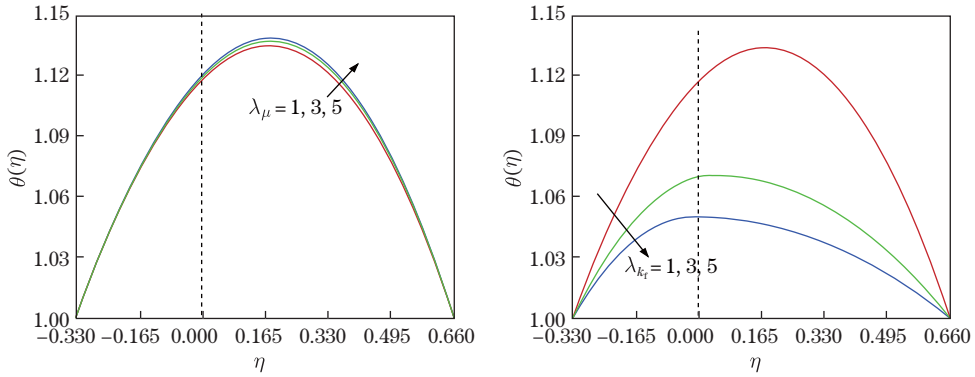

Fig. 9 Variation in temperature field with change in the physical ratios λ_μ and λ_{k_f} in case of $\zeta_1 = \zeta_2 = 1$, $H_1 = 1$, $H_2 = 2$, $Ha_1 = 3$, $S_{e1} = \Omega_1 = 1$, $Br_1 = 0.1$, and $N_{t1} = N_{B1} = 1$ (color online)

The variations of the skin friction coefficient C_{fi} and the Nusselt number Nu_i with κ_1 and Hartman number are presented in Fig. 10 and Fig. 11, respectively. It is known that the flow velocity is a key factor to determine the skin friction so that its variation has distinct effects on C_{fi} as well. It has been already known from Fig. 4 that the flow rate increases near both channel walls as κ_1 evolves. This trend is also found for the variation of C_{fi}, but the direction on the upper wall is opposite to that on the lower wall. It can also be seen that the trend in the change of local skin friction coefficient with respect to the Hartman number changes at $Ha_1 = 1$. When $Ha_1 < 1$, the local skin friction increases for smaller values of κ_1, but as κ_1 increases, this change becomes negligible. On the other hand, for $Ha_1 > 1$, the local skin friction has a negligible increase with increase in Ha_1 but as κ_1 increases, this trend reverses and the local skin friction has a decreasing trend. This is due to the fact that the lateral electric field considered in this study is small. Hence, the opposing force from the electric field is greater as compared with the aiding force in case of $Ha_1 > 1$.

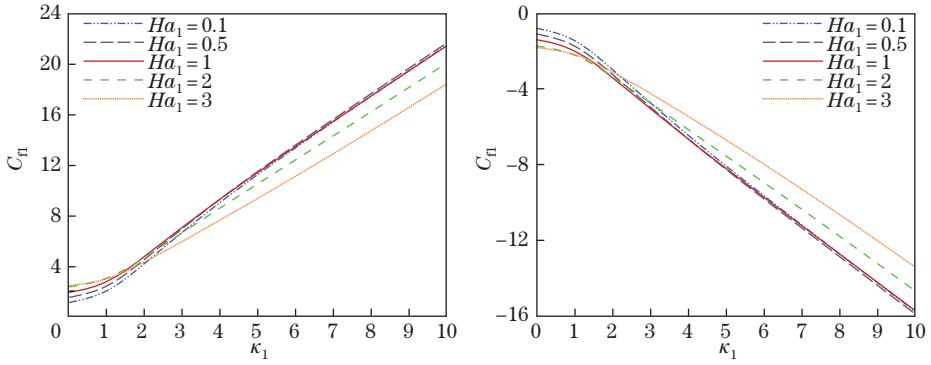

Fig. 10 Variation of local skin friction coefficient with change in the electro-osmotic parameter κ_1 and Hartman number in case of $\zeta_1 = \zeta_2 = 1$, $H_1 = 1$, $H_2 = 2$, $S_{e1} = \Omega_1 = 1$, $Br_1 = 0.1$, and $N_{t1} = N_{B1} = 0.1$ (color online)

In Fig. 11, the Nusselt number decreases on the upper wall but increases on the lower wall with increase in κ_1. This is because the coordinates are set at the interface of the two layers so that the signs on the upper and lower walls are just opposite. Physically, this ratio decreases as κ_1 increases since the EDL effect is weakened and the fluid motion accelerates. Therefore, the heat conduction increases more quickly than the heat convection owing to this change. On the other hand, the Nusselt number increases with increase in the Hartman number. This increase is due to the increase of thermal convection owing to a decrease in the viscous force as a consequence of higher values of Ha_1.

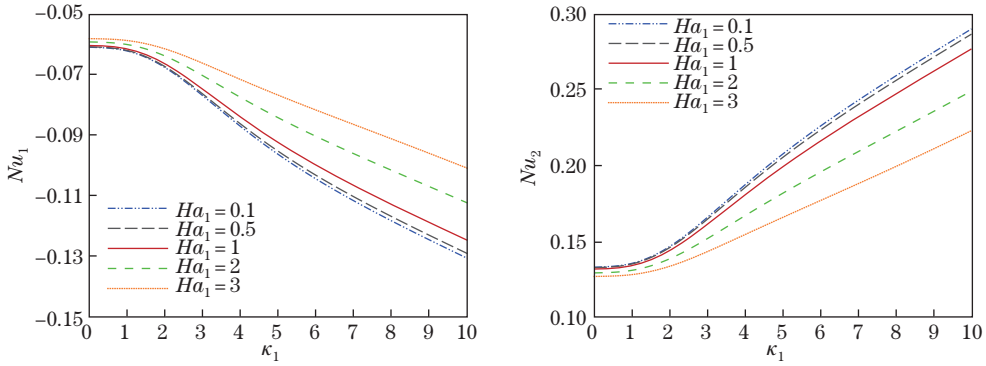

Fig. 11 Variation of Nusselt number with change in the electro-osmotic parameter κ_1 and Hartman number in case of $\zeta_1 = \zeta_2 = 1$, $H_1 = 1$, $H_2 = 2$, $S_{e1} = \Omega_1 = 1$, $Br_1 = 0.1$, and $N_{t1} = N_{B1} = 0.1$ (color online)

The evolution of the entropy analysis is presented in Figs. 12–14 for different scenarios. The total entropy S_{total} in the channel is associated with different parameters including the

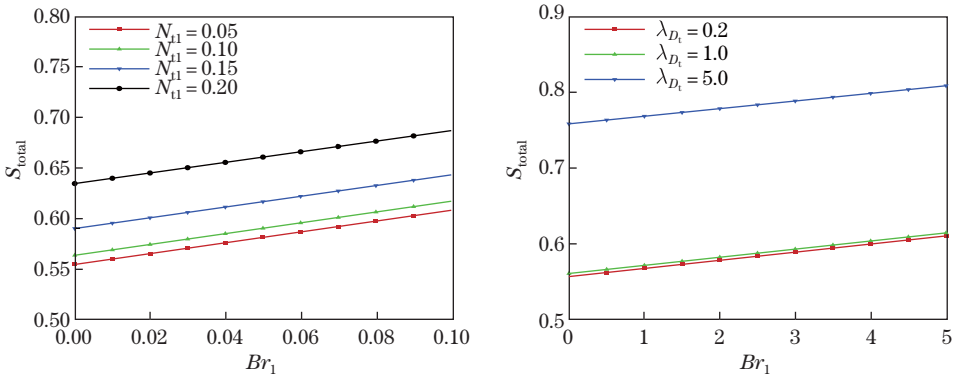

Fig. 12 Variation of the total entropy S_{total} with the Brinkman number Br_1 while changing the thermophoretic diffusion parameter N_{t1} and ratio λ_{D_t} in case of $\zeta_1 = \zeta_2 = 1$, $H_1 = 1$, $H_2 = 2$, $Ha_1 = S_{e1} = \Omega_1 = \kappa_1 = 1$, $N_{B1} = 0.1$, and $N_{t1} = 0.1$ for the right side (color online)

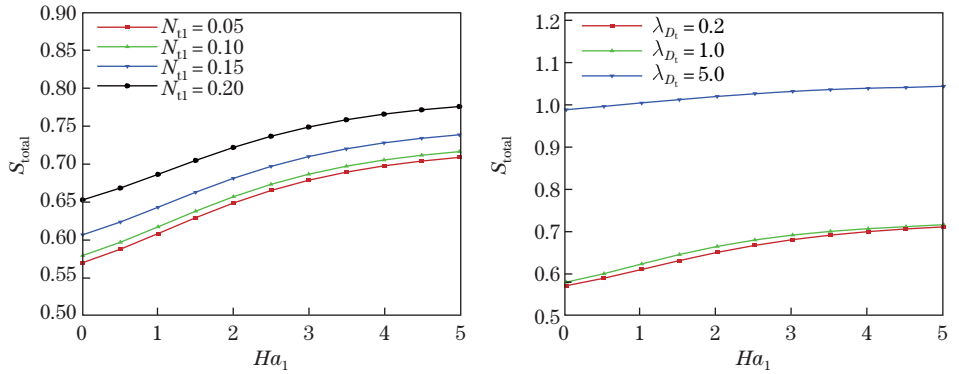

Fig. 13 Variation of the total entropy S_{total} with the Hartman number Ha_1 while changing the thermophoretic diffusion parameter N_{t1} and ratio λ_{D_t} in case of $\zeta_1 = \zeta_2 = 1$, $H_1 = 1$, $H_2 = 2$, $S_{e1} = \Omega_1 = \kappa_1 = 1$, $Br_1 = 0.1$, $N_{B1} = 0.1$, and $N_{t1} = 0.1$ for the right side (color online)

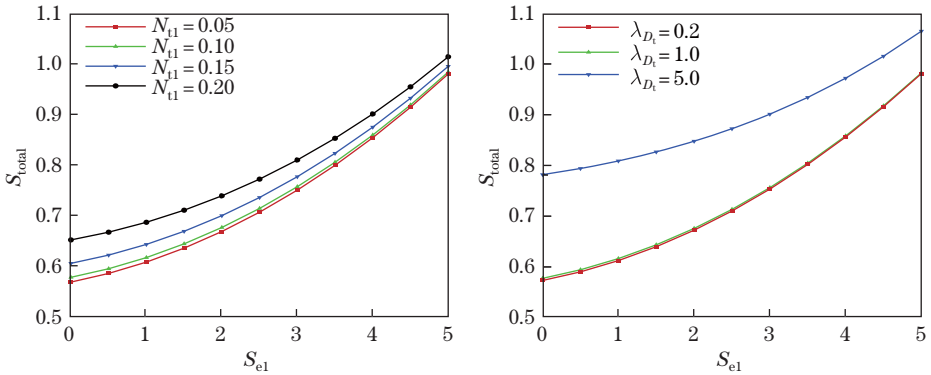

Fig. 14 Variation of the total entropy S_{total} with the electric field parameter S_{e1} while changing the thermophoretic diffusion parameter N_{t1} and ratio λ_{D_t} in case of $\zeta_1 = \zeta_2 = 1$, $H_1 = 1$, $H_2 = 2$, $Ha_1 = \Omega_1 = \kappa_1 = 1$, $Br_1 = 0.1$, $N_{B1} = 0.1$, and $N_{t1} = 0.1$ for the right side (color online)

thermophoresis parameter N_{t1}, the thermophoresis diffusion ratio λ_{D_t}, the Brinkman number Br_1, the Hartman number Ha_1 and the electric field strength parameter S_{e1}. It is seen in Fig. 12 that S_{total} enhances with increase in Br_1 for a specific value of N_{t1} (or λ_{D_t}). Similarly, S_{total} increases with increase in N_{t1} (or λ_{D_t}) when Br_1 is kept at a constant value. In the latter case, this increasing trend becomes more evident. Figure 13 shows the changing trend of S_{total} with Ha_1, S_{total} increases rapidly at first, after a significant increase in Ha_1, the growing of S_{total} becomes insignificant. While as Ha_1 is kept constant, S_{total} increases with increase in N_{t1} (or λ_{D_t}) as well. As shown in Fig. 14, S_{e1} has a similar effect on S_{total} which increases as S_{e1} increases for a specific value of N_{t1} (or λ_{D_t}) or vice versa.

6 Conclusions

The fully developed steady immiscible two-layer flow of nanofluids in a micro-channel in the presence of electro-kinetic effects has been studied. Buongiorno's model[49] has been applied for modelling the behavior of nanofluids. The conservation equations embodying the total mass, momentum, thermal energy and nanoparticle volume fraction have been reduced into a group of ordinary differential equations via appropriate similarity transformations. The consequent system of those coupled equations has been solved analytically by means of the HAM. Highly accurate analytical approximations for the electric potential, velocity, temperature and nanoparticle volume fraction have been obtained. Important physical quantities and entropy generation have been analyzed and discussed. A comparison has been made to determine the significance of EDL effects in the presence of an external electric field. The major findings of this work are summarized as follows:

(i) Buongiorno's model[49] is extended to describe two-layer nanofluids' flow in a micro-channel with EDL effects.

(ii) Analytical solution is obtained for the electrostatic potential.

(iii) Effects of various physical parameters on distributions of electrostatic potential, velocity field, temperature distribution and nanoparticle volume fraction are graphically presented and physically explained.

(iv) Although EDL effects are negligibly small in the presence of an external electric field, these effects decrease with increase in the electro-osmotic parameter. This analysis supports the findings by Zhao et al.[43].

(v) Thermophoresis diffusion has significant effects on behaviors of two-layer nanofluids' flow in a micro-channel.

(vi) Viscosity in a micro-channel is a significant factor that is needed to be considered.

(vii) Evolution of total entropy analysis in a two-layer micro-channel is performed. The changes in total entropy generation of the system with respect to the Hartman number and Brinkman number follow the trends highlighted by Xie and Jian[42]. Whereas, the total entropy increases when either of the thermophoretic diffusion parameter or electric field strength parameter is increased.

References

[1] GRAVESEN, P., BRANEBJERG, J., and JENSEN, O. S. Microfluidics —– a review. *Journal of Micromechanics and Microengineering*, **3**(4), 168–182 (1993)

[2] BECKER, H. and GÄRTNER, C. Polymer microfabrication methods for microfluidic analytical applications. *Electrophoresis*, **21**(1), 12–26 (2000)

[3] ZIAIE, B., BALDI, A., LEI, M., GU, Y., and SIEGEL, R. A. Hard and soft micromachining for BioMEMS: review of techniques and examples of applications in microfluidics and drug delivery. *Advanced Drug Delivery Reviews*, **56**(2), 145–172 (2004)

[4] NGUYEN, N. T. and WU, Z. Micromixers —— a review. *Journal of Micromechanics and Microengineering*, **15**(2), R1–R16 (2004)

[5] OHNO, K. I., TACHIKAWA, K., and MANZ, A. Microfluidics: applications for analytical purposes in chemistry and biochemistry. *Electrophoresis*, **29**(22), 4443–4453 (2008)

[6] MAXWELL, J. C. *A Treatise on Electricity and Magnetism*, Clarendon Press, Oxford (1873)

[7] CHOI, S. U. and EASTMAN, J. A. Enhancing thermal conductivity of fluids with nanoparticles. *ASME International Mechanical Engineering Congress and Exposion*, 12–17 (1995)

[8] EASTMAN, J. A., CHOI, S. U. S., LI, S., YU, W., and THOMPSON, L. J. Anomalously increased effective thermal conductivities of ethylene glycol-based nanofluids containing copper nanoparticles. *Applied Physics Letters*, **78**(6), 718–720 (2001)

[9] XUAN, Y. and LI, Q. Investigation on convective heat transfer and flow features of nanofluids. *Journal of Heat Transfer*, **125**(1), 151–155 (2003)

[10] HERIS, S. Z., ETEMAD, S. G., and ESFAHANY, M. N. Experimental investigation of oxide nanofluids laminar flow convective heat transfer. *International Communications in Heat and Mass Transfer*, **33**(4), 529–535 (2006)

[11] WILLIAMS, W., BUONGIORNO, J., and HU, L. W. Experimental investigation of turbulent convective heat transfer and pressure loss of alumina/water and zirconia/water nanoparticle colloids (nanofluids) in horizontal tubes. *Journal of Heat Transfer*, **130**(4), 042412 (2008)

[12] KUZNETSOV, A. V. and NIELD, D. A. Natural convective boundary-layer flow of a nanofluid past a vertical plate. *International Journal of Thermal Sciences*, **49**(2), 243–247 (2010)

[13] WANG, X. J., LI, X. F., XU, Y. H., and ZHU, D. S. Thermal energy storage characteristics of Cu-H_2O nanofluids. *Energy*, **78**, 212–217 (2014)

[14] MANIKANDAN, S. and RAJAN, K. S. MgO-therminol 55 nanofluids for efficient energy management: analysis of transient heat transfer performance. *Energy*, **88**, 408–416 (2015)

[15] KARIMIPOUR, A., NEZHAD, A. H., DORAZIO, A., ESFE, M. H., SAFAEI, M. R., and SHIRANI, E. Simulation of copper–water nanofluid in a microchannel in slip flow regime using the lattice Boltzmann method. *European Journal of Mechanics-B/Fluids*, **49**, 89–99 (2015)

[16] HUNTER, R. J. *Zeta Potential in Colloid Science: Principles and Applications*, Academic Press, Harcour Brace Jovanovich (2013)

[17] MALA, G. M., LI, D., and DALE, J. D. Heat transfer and fluid flow in microchannels. *International Journal of Heat and Mass Transfer*, **40**, 3079–3088 (1997)

[18] MALA, G. M. and LI, D. Flow characteristics of water in microtubes. *International Journal of Heat and Fluid Flow*, **20**(2), 142–148 (1999)

[19] REN, L. Q., QU, W. L., and LI, D. Q. Interfacial electrokinetic effects on liquid flow in microchannels. *International Journal of Heat and Mass Transfer*, **44**(16), 3125–3134 (2001)

[20] DARABI, J. and EKULA, K. Development of a chip-integrated micro cooling device. *Microelectronics Journal*, **34**(11), 1067–1074 (2003)

[21] DONALDSON, L. Small and powerful nuclear battery developed. *Materials Today*, **12**(11), 10–10 (2009)

[22] WANG, B. X. and PENG, X. F. Experimental investigation on liquid forced-convection heat transfer through microchannels. *International Journal of Heat and Mass Transfer*, **37**, 73–82 (1994)

[23] GUO, Z. Y. and LI, Z. X. Size effect on single-phase channel flow and heat transfer at microscale. *International Journal of Heat and Fluid Flow*, **24**(3), 284–298 (2003)

[24] REN, C. L. and LI, D. Improved understanding of the effect of electrical double layer on pressure-driven flow in microchannels. *Analytica Chimica Acta*, **531**(1), 15–23 (2005)

[25] YOU, X. Y. and GUO, L. X. Analysis of EDL effects on the flow and flow stability in microchannels. *Journal of Hydrodynamics*, **22**(5), 725–731 (2010)

[26] JING, D., PAN, Y., and WANG, X. Joule heating, viscous dissipation and convective heat transfer of pressure-driven flow in a microchannel with surface charge-dependent slip. *International Journal of Heat and Mass Transfer*, **108**, 1305–1313 (2017)

[27] SRINIVAS, B. Electroosmotic flow of a power law fluid in an elliptic microchannel. *Colloids and Surfaces A*: *Physicochemical and Engineering Aspects*, **492**, 144–151 (2016)

[28] QI, C. and NG, C. O. Electroosmotic flow of a two-layer fluid in a slit channel with gradually varying wall shape and zeta potential. *International Journal of Heat and Mass Transfer*, **119**, 52–64 (2018)

[29] ZHENG, J. and JIAN, Y. Rotating electroosmotic flow of two-layer fluids through a microparallel channel. *International Journal of Mechanical Sciences*, **136**, 293–302 (2018)

[30] TAO, L. N. On combined free and forced convection in channels. *Journal of Heat Transfer*, **82**(3), 233–238 (1960)

[31] AUNG, W. and WORKU, G. Developing flow and flow reversal in a vertical channel with asymmetric wall temperatures. *Journal of Heat Transfer*, **108**(2), 299–304 (1986)

[32] KUBAN, P., DASGUPTA, P. K., and MORRIS, K. A. Microscale continuous ion exchanger. *Analytical Chemistry*, **74**(21), 5667–5675 (2002)

[33] KAMHOLZ, A. E., WEIGL, B. H., FINLAYSON, B. A., and YAGER, P. Quantitative analysis of molecular interaction in a microfluidic channel: the T-sensor. *Analytical Chemistry*, **71**(23), 5340–5347 (1999)

[34] WEIGL, B. H., BARDELL, R. L., KESLER, N., and MORRIS, C. J. Lab-on-a-chip sample preparation using laminar fluid diffusion interfaces-computational fluid dynamics model results and fluidic verification experiments. *Fresenius' Journal of Analytical Chemistry*, **371**(2), 97–105 (2001)

[35] BRASK, A., GORANOVIC, G., and BRUUS, H. *Electroosmotic Pumping of Nonconducting Liquids by Viscous Drag from a Secondary Conducting Liquid*, Nanotech, 190–193 (2003)

[36] GAO, Y., WONG, T. N., YANG, C., and OOI, K. T. Two-fluid electroosmotic flow in microchannels. *Journal of Colloid and Interface Science*, **284**(1), 306–314 (2005)

[37] SHANKAR, V. and SHARMA, A. Instability of the interface between thin fluid films subjected to electric fields. *Journal of Colloid and Interface Science*, **274**(1), 294–308 (2004)

[38] VERMA, R., SHARMA, A., KARGUPTA, K., and BHAUMIK, J. Electric field induced instability and pattern formation in thin liquid films. *Langmuir*, **21**(8), 3710–3721 (2005)

[39] GAO, Y., WANG, C., WONG, T. N., YANG, C., NGUYEN, N. T., and OOI, K. T. Electroosmotic control of the interface position of two-liquid flow through a microchannel. *Journal of Micromechanics and Microengineering*, **17**(2), 358–366 (2007)

[40] GAIKWAD, H., BASU, D. N., and MONDAL, P. K. Electroosmotic transport of immiscible binary system with a layer of non-conducting fluid under interfacial slip: the role applied pressure gradient. *Electrophoresis*, **37**(14), 1998–2009 (2016)

[41] GAIKWAD, H. S., BASU, D. N., and MONDAL, P. K. Slip driven micro-pumping of binary system with a layer of non-conducting fluid under electrical double layer phenomenon. *Colloids and Surfaces A*: *Physicochemical and Engineering Aspects*, **518**, 166–172 (2017)

[42] XIE, Z. Y. and JIAN, Y. J. Entropy generation of two-layer magnetohydrodynamic electroosmotic flow through microparallel channels. *Energy*, **139**, 1080–1093 (2017)

[43] ZHAO, Q., XU, H., and TAO, L. Nanofluid flow and heat transfer in a microchannel with interfacial electrokinetic effects. *International Journal of Heat and Mass Transfer*, **124**, 158–167 (2018)

[44] BEJAN, A. A study of entropy generation in fundamental convective heat transfer. *Journal of Heat Transfer*, **101**(4), 718–725 (1979)

[45] BEJAN, A. Second law analysis in heat transfer. *Energy*, **5**(8-9), 720–732 (1980)

[46] ABBASSI, H. Entropy generation analysis in a uniformly heated microchannel heat sink. *Energy*, **32**(10), 1932–1947 (2007)

[47] MAKINDE, O. D. Entropy-generation analysis for variable-viscosity channel flow with non-uniform wall temperature. *Applied Energy*, **85**(5), 384–393 (2008)

[48] XU, H., RAEES, A., and XU, X. H. Entropy generation of nanofluid flow and heat transfer driven through a paralleled microchannel. *Canadian Journal of Physics*, **97**(6), 678–691 (2018)

[49] BUONGIORNO, J. Convective transport in nanofluids. *Journal of Heat Transfer*, **128**(3), 240–250 (2006)

[50] FAROOQ, U. and LIN,Z. L. Nonlinear heat transfer in a two-layer flow with nanofluids by OHAM. *Journal of Heat Transfer*, **136**(2), 021702 (2014)

[51] FAROOQ, U., HAYAT, T., ALSAEDI, A., and LIAO, S. J. Heat and mass transfer of two-layer flows of third-grade nano-fluids in a vertical channel. *Applied Mathematics and Computation*, **242**, 528–540 (2014)

[52] LIAO, S. J. *Homotopy Analysis Method in Nonlinear Differential Equations*, Higher Education Press, Beijing, 153–165 (2012)

[53] DAUENHAUER, E. C. and MAJDALANI, J. Exact self-similarity solution of the Navier-Stokes equations for a porous channel with orthogonally moving walls. *Physics of Fluids*, **151**, 1485–1495 (2003)

[54] SUN, Q. and POP, I. Free convection in a triangle cavity filled with a porous medium saturated with nanofluids with flush mounted heater on the wall. *International Journal of Thermal Sciences*, **50**(11), 2141–2153 (2011)

[55] NGUYEN, N. T. Micro-magnetofluidics: interactions between magnetism and fluid flow on the microscale microfluid. *Microfluids and Nanofluids*, **12**, 1–16 (2012)

[56] SARKAR, S., GANGULY, S., and CHAKRABORTY, S. Influence of combined electromagneto-hydrodynamics on microchannel flow with electrokinetic effect and interfacial slip. *Microfluidics and Nanofluidics*, **21**, 1–16 (2017)

Appendix A

In the framework of the HAM, it is of importance to construct the HAM deformation equation,

$$(1-q)\mathcal{L}_\Psi(\Psi(\eta;q)-\varphi_0(\eta))=q\hbar_\Psi\mathcal{N}_\Psi(\Psi(\eta;q)), \tag{A1}$$

where $\mathcal{L}_\Psi$ is the linear operator, $\mathcal{N}_\Psi$ is the nonlinear operator, $\Psi(\eta;q)$ is the mapping function of $\varphi(\eta)$, $q\in[0,1]$ is an embedding parameter, and $\hbar_\Psi$ is the convergence-control parameter.

The mth-order deformation equation is obtained, by differentiating Eq. (A1) m times with respect to q, then dividing by $m!$, finally setting $q=0$, as

$$\mathcal{L}_\Psi(\varphi_m(\eta)-\chi_m\varphi_0(\eta))=\hbar_\Psi R_m(\eta), \tag{A2}$$

where

$$\varphi_m(\eta)=\frac{1}{m!}\frac{\partial^m\hat{\phi}(\eta;q)}{\partial q^m}\Big|_{q=0},\quad R_m(\eta)=\frac{1}{m!}\frac{\partial^{m-1}\mathcal{N}[\Psi(\eta q)]}{\partial q^{m-1}}\Big|_{q=0}, \tag{A3}$$

and

$$\chi_m=\begin{cases}0, & m\leqslant 1,\\ 1, & m>1.\end{cases} \tag{A4}$$

In application of the HAM technique into our problem, the linear operators for Eqs. (20)–(27) are chosen as

$$\mathcal{L}=\frac{\partial^2}{\partial\eta^2}. \tag{A5}$$

The initial guesses for the computations are given as

$$\begin{cases}\phi_{1,0}(\eta)=\dfrac{\lambda_\varepsilon\eta(\zeta_2-\zeta_1)}{\lambda_\varepsilon h_1+h_2}+\dfrac{h_2\zeta_1+\lambda_\varepsilon h_1\zeta_2}{\lambda_\varepsilon h_1+h_2},\\ \phi_{2,0}(\eta)=\dfrac{\eta(\zeta_2-\zeta_1)}{\lambda_\varepsilon h_1+h_2}+\dfrac{h_2\zeta_1+\lambda_\varepsilon h_1\zeta_2}{\lambda_\varepsilon h_1+h_2},\\ u_{1,0}(\eta)=u_{2,0}(\eta)=0,\\ \theta_{1,0}(\eta)=\theta_{2,0}(\eta)=s_{1,0}(\eta)=s_{2,0}(\eta)=1.\end{cases} \tag{A6}$$

Solutions to $\phi_i(\eta)$, $u_i(\eta)$, $\theta_i(\eta)$, and $s_i(\eta)$ are expanded in the following forms:

$$\begin{cases} \phi_i = \phi_{i,0} + \sum\limits_{j=1}^{\infty} \phi_{i,j}, \quad u_i = u_{i,0} + \sum\limits_{j=1}^{\infty} u_{i,j}, \\ s_i = s_{i,0} + \sum\limits_{j=1}^{\infty} s_{i,j}, \quad \theta_i = \theta_{i,0} + \sum\limits_{j=1}^{\infty} \theta_{i,j}. \end{cases} \tag{A7}$$

The mth order HAM deformation equations can be written as

$$\begin{cases} \phi''_{i,m} - \chi_m \phi''_{i,m-1} = \hbar_{\phi_i} R_{\phi_{i,m}}, \quad u''_{i,m} - \chi_m u''_{i,m-1} = \hbar_{u_i} R_{u_{i,m}}, \\ \theta''_{i,m} - \chi_m \theta''_{i,m-1} = \hbar_{\theta_i} R_{\theta_{i,m}}, \quad s''_{i,m} - \chi_m s''_{i,m-1} = \hbar_{s_i} R_{s_{i,m}} \end{cases} \tag{A8}$$

subject to the boundary conditions

$$\begin{cases} \eta = -h_1: & \phi_{1,m} = u_{1,m} = \theta_{1,m} = s_{1,m} = 0, \\ \eta = 0: & \begin{cases} \phi_{1,m} = \phi_{2,m}, \quad u_{1,m} = \dfrac{\lambda_\varepsilon}{\lambda_\mu} u_{2,m}, \quad \theta_{1,m} = \theta_{2,m}, \\ s_{1,m} = s_{2,m}, \quad \phi'_{1,m} = \lambda_\varepsilon \phi'_{2,m}, \quad u'_{1,m} = \lambda_\varepsilon u'_{2,m}, \\ N_{\mathrm{B}1}(s'_{1,m} - \lambda_{D_\mathrm{B}} s'_{2,m}) + N_{\mathrm{t}1}(\theta'_{1,m} - \lambda_{D_\mathrm{t}} \theta'_{2,m}) = 0, \\ \theta'_{1,m} = \lambda_{k_\mathrm{f}} \theta'_{2,m}, \end{cases} \\ \eta = h_2: & \phi_{2,m} = u_{2,m} = \theta_{2,m} = s_{2,m} = 0, \end{cases} \tag{A9}$$

where $\hbar_{\phi_i}$, $\hbar_{u_i}$, $\hbar_{\theta_i}$, and $\hbar_{s_i}$ $(i = 1, 2)$ are the respective convergence control parameters and $R_{\phi_{i,m}}$, $R_{u_{i,m}}$, $R_{\theta_{i,m}}$, and $R_{s_i,m}$, for $i = 1, 2$, are defined as

$$R_{\phi_{1,m}} = \phi''_{1,m-1} - \kappa_1^2 \phi_{1,m-1}, \tag{A10}$$

$$R_{\Phi_{2,m}} = \phi''_{2,m-1} - \kappa_2^2 \phi_{2,m-1}, \tag{A11}$$

$$R_{u_{1,m}} = u''_{1,m-1} - Ha_1^2 u_{1,m-1} + \kappa_1^2 \phi_{1,m-1} + (1 - \chi_m)(S_{\mathrm{e}1} Ha_1 + \Gamma_1), \tag{A12}$$

$$R_{u_{2,m}} = u''_{2,m-1} - Ha_2^2 u_{2,m-1} + \kappa_2^2 \phi_{2,m-1} + (1 - \chi_m)(S_{\mathrm{e}2} Ha_2 + \Gamma_2), \tag{A13}$$

$$\begin{aligned} R_{\theta_{1,m}} = {} & \theta''_{1,m-1} + \sum_{j=0}^{m-1} (N_{\mathrm{B}1} \theta'_{1,j} s'_{1,m-1-j} + N_{\mathrm{t}1} \theta'_{1,j} \theta'_{1,m-1-j}) \\ & + \sum_{j=0}^{m-1} (Br_1 u'_{1,j} u'_{1,m-1-j} + Br_1 Ha_1^2 u_{1,j} u_{1,m-1-j}) \\ & + (1 - \chi_m)\Omega_1 - 2S_{\mathrm{e}1} Br_1 Ha_1 u_{1,m-1}, \end{aligned} \tag{A14}$$

$$\begin{aligned} R_{\theta_{2,m}} = {} & \theta''_{2,m-1} + \sum_{j=0}^{m-1} (N_{\mathrm{B}2} \theta'_{2,j} s'_{2,m-1-j} + N_{\mathrm{t}2} \theta'_{2,j} \theta'_{2,m-1-j}) \\ & + \sum_{j=0}^{m-1} (Br_2 u'_{2,j} u'_{2,m-1-j} + Br_2 Ha_2^2 u_{2,j} u_{2,m-1-j}) \\ & + (1 - \chi_m)\Omega_2 - 2S_{\mathrm{e}2} Br_2 Ha_2 u_{2,m-1}, \end{aligned} \tag{A15}$$

$$R_{s_{1,m}} = s''_{1,m-1} + \frac{N_{\mathrm{t}1}}{N_{\mathrm{B}1}} \theta''_{1,m-1}, \tag{A16}$$

$$R_{s_{2,m}} = s''_{2,m-1} + \frac{N_{\mathrm{t}2}}{N_{\mathrm{B}2}} \theta''_{2,m-1}. \tag{A17}$$

The solutions to Eq. (A8) are expressed as follows:

$$\phi_{1,m}(\eta) = \phi_1^*(\eta) + \chi_m \phi_{1,m-1}(\eta) + C_{1,m} + C_{2,m}\eta, \tag{A18}$$
$$\phi_{2,m}(\eta) = \phi_2^*(\eta) + \chi_m \phi_{2,m-1}(\eta) + C_{3,m} + C_{4,m}\eta, \tag{A19}$$
$$u_{1,m}(\eta) = u_1^*(\eta) + \chi_m u_{1,m-1}(\eta) + C_{5,m} + C_{6,m}\eta, \tag{A20}$$
$$u_{2,m}(\eta) = u_2^*(\eta) + \chi_m u_{2,m-1}(\eta) + C_{7,m} + C_{8,m}\eta, \tag{A21}$$
$$\theta_{1,m}(\eta) = \theta_1^*(\eta) + \chi_m \theta_{1,m-1}(\eta) + C_{9,m} + C_{10,m}\eta, \tag{A22}$$
$$\theta_{2,m}(\eta) = \theta_2^*(\eta) + \chi_m \theta_{2,m-1}(\eta) + C_{11,m} + C_{12,m}\eta, \tag{A23}$$
$$s_{1,m}(\eta) = s_1^* + \chi_m s_{1,m-1}(\eta) + C_{13,m} + C_{14,m}\eta, \tag{A24}$$
$$s_{2,m}(\eta) = s_2^* + \chi_m s_{2,m-1}(\eta) + C_{15,m} + C_{16,m}\eta, \tag{A25}$$

where $\phi_{i,m}^*(\eta)$, $u_{i,m}^*(\eta)$, $\theta_{i,m}^*(\eta)$, and $s_{i,m}^*(\eta)$ are particular solutions, defined by

$$\begin{cases} \phi_i^* = \mathcal{L}^{-1}[\hbar_{\phi_i} R_{\phi_{i,m}}], & u_i^* = \mathcal{L}^{-1}[\hbar_{u_i} R_{u_{i,m}}], \\ \theta_i^* = \mathcal{L}^{-1}[\hbar_{\theta_i} R_{\theta_{i,m}}], & s_i^* = \mathcal{L}^{-1}[\hbar_{s_i} R_{s_{i,m}}], \end{cases} \tag{A26}$$

where $\mathcal{L}^{-1}$ is the inverse linear operator, which holds the following properties:

$$\mathcal{L}^{-1}[c_0\eta^m] = \frac{c_0\eta^m}{(m+2)(m+1)}, \quad \mathcal{L}^{-1}[a_0(\eta) + b_0(\eta)] = \mathcal{L}^{-1}[a_0(\eta)] + \mathcal{L}^{-1}[b_0(\eta)]. \tag{A27}$$

The constants $C_{i,m}$, $i = 1, 2, \cdots, 16$ defined in Eqs. (A18) to (A25) can be obtained using the boundary conditions (A9).

Appendix B

$$E_{\phi_1}(m) = \int_{-h_1}^{0} (\phi_1'' - \kappa_1^2 \phi_1)^2 \mathrm{d}\eta, \tag{A28}$$
$$E_{\phi_2}(m) = \int_{0}^{h_2} (\phi_2'' - \kappa_2^2 \phi_2)^2 \mathrm{d}\eta, \tag{A29}$$
$$E_{u_1}(m) = \int_{-h_1}^{0} (u_1'' - Ha_1^2 u_1 + S_{\mathrm{e}1} Ha_1 + \Gamma_1 + \kappa_1^2 \phi_1)^2 \mathrm{d}\eta, \tag{A30}$$
$$E_{u_2}(m) = \int_{0}^{h_2} (u_2'' - Ha_2^2 u_2 + S_{\mathrm{e}2} Ha_2 + \Gamma_2 + \kappa_2^2 \phi_2)^2 \mathrm{d}\eta, \tag{A31}$$
$$E_{\theta_1}(m) = \int_{-h_1}^{0} (\theta_1'' + N_{\mathrm{B}1}\theta_1' s_1' + N_{\mathrm{t}1}\theta_1'^2 + Br_1(u_1'^2 + Ha_1^2 u_1^2 - 2S_{\mathrm{e}1} Ha_1 u_1) + \Omega_1)^2 \mathrm{d}\eta, \tag{A32}$$
$$E_{\theta_2}(m) = \int_{0}^{h_2} (\theta_2'' + N_{\mathrm{B}2}\theta_2' s_2' + N_{\mathrm{t}2}\theta_2'^2 + Br_2(u_2'^2 + Ha_2^2 u_2^2 - 2S_{\mathrm{e}2} Ha_2 u_2) + \Omega_2)^2 \mathrm{d}\eta, \tag{A33}$$
$$E_{s_1}(m) = \int_{-h_1}^{0} \left(s_1'' + \frac{N_{\mathrm{t}1}}{N_{\mathrm{B}1}}\theta_1''\right)^2 \mathrm{d}\eta, \tag{A34}$$
$$E_{s_2}(m) = \int_{0}^{h_2} \left(s_2'' + \frac{N_{\mathrm{t}2}}{N_{\mathrm{B}2}}\theta_2''\right)^2 \mathrm{d}\eta. \tag{A35}$$